




Physical, optical, and advanced radiation absorption characteristics of cadmium lead phosphate glasses containing MoO₃

Kh. S. Shaaban^{1,*} , Ateyyah M. Al-Baradi², and Atif Mossad Ali^{3,4}

¹Chemistry Department, Faculty of Science, Al-Azhar University, P.O. Box 71524, Assiut, Egypt

²Department of Physics, College of Science, Taif University, P.O. Box 11099, Taif 21944, Saudi Arabia

³Physics Department, Faculty of Science, King Khalid University, Abha 61413, Saudi Arabia

⁴Department of Physics, Faculty of Science, Assiut University, Assiut 71516, Egypt

Received: 30 October 2021

Accepted: 3 December 2021

Published online:

27 January 2022

© The Author(s), under exclusive licence to Springer Science+Business Media, LLC, part of Springer Nature 2021

ABSTRACT

In glasses with the composition $45\text{P}_2\text{O}_5-45\text{PbO}_2-(10-x)\text{CdO}-x\text{MoO}_3$, $x = (0 \leq x \leq 5 \text{ mol}\%)$, melt quenching technique was used to fabricate these samples. The structural characteristics of the proposed glasses were determined using X-ray diffraction. Fabricated glasses were found to have a higher density and refractive index. The spectroscopic characteristics of fabricated glasses were evaluated using UV–VIs. Energy bandgap increases as the content of MoO₃ increases, while Urbach energy decreases. Phy-X/PSD has been used to investigate radiation shielding properties. Mass attenuation coefficient values are positively affected by increases in the MoO₃ ratio. G1 has the maximum half-value layer value, whereas G5 has the minimum. The exposure and energy absorption build-up factor (EBF and EABF) values decreased slightly as the MoO₃ content increased. As a result, among all other glasses, G5 glasses have the best shielding capacity.

1 Introduction

MoO₃ is not a glass-forming oxide on its own, but it can combine with other glass-forming oxides as P₂O₅ to form glasses. Recently, several glass systems involving P₂O₅ and MoO₃ were investigated [1–4]. IR spectroscopy has been extensively used for structural characterization of MoO₃–P₂O₅ glasses [5]. Selvaraj and Rao [3] investigated PbO–MoO₃–P₂O₅ glasses. Because of PbO's ability to act as a modifier with the

structural units of PbO₆, adding PbO to phosphate glass increases the glass's stability against devitrification and causes the glass to become chemically inactive [6].

Incorporating transition metal oxide (TMO) to glass improves electronic characteristics by allowing electrons to transfer between valence states. The physical and mechanical characteristics of the glass are improved dramatically by CdO. The physical and

Address correspondence to E-mail: khamies1078@yahoo.com

chemical properties of glass systems with oxidation states 4 or 6 (CdO_4 or CdO_6) are altered by CdO [6–9].

Many industries, such as medical physics and nuclear research, can benefit from nuclear technologies. The interaction of X-ray radiation and a neutron with the material is critical in a variety of radiation technologies and applications. Therefore, radiation shielding has gotten a lot of press. The appropriate precursors for radiation shielding could be specific glass compositions. Glass materials have a range of excellent compositional properties that make them suitable for these applications [10–13].

Over the last few decades, researchers have investigated several types of glasses for use as alternative shield materials in a variety of nuclear applications. In extension to their ability to absorb high-energy photons, they have a variety of intriguing physical characteristics like transparency, ease of preparation, and stability when exposed to an external field.

The authors of this article investigate the use of fabricated glasses in radiation shielding applications. These glasses have excellent optical characteristics and can be used as radiation shields. Some physical and radiation shielding features were evaluated to achieve this goal.

2 Materials and methods

The chemical composition of the materials used to fabricate glass samples is shown in Table 1. In the following reaction, five lead, phosphate-based glass samples were manufactured. $\text{PbO}_2 + \text{CdO} + \text{MoO}_3 + 2(\text{NH}_4)_2\text{HPO}_4 \xrightarrow[-(4\text{NH}_3+3\text{H}_2\text{O})]{\Delta} (\text{PbO}_2 + \text{CdO} + \text{MoO}_3 + \text{P}_2\text{O}_5) \rightarrow \text{glass samples}$. The classic melt quenching method was used to produce the glasses,

Table 1 Fabricated glasses with mol%

Code	mol%			
	P_2O_5	PbO_2	CdO	MoO_3
G1	45	45	10	0
G2	45	45	9	1
G3	45	45	8	2
G4	45	45	7	3
G5	45	45	5	5

which took 45 min at 1100 °C. To relieve thermal stress, the fabricated glasses were annealed at 400 °C for 2 h and then cooled gradually.

XRD patterns on a Rigaku-Top XRD were used to check the condition of the glasses. The spectrophotometer type (JASCO V-670) recorded UV–VIS–NIR spectra in the range of 2700–200 nm. The study's goal was achieved by estimating all effective parameters that judge the shielding effectiveness of the prepared glasses using the online version of the Phy-X/PSD software. These glasses were studied for their (MAC), (LAC), and (HVL). We calculated and discussed EBF and EABF.

3 Results and discussion

3.1 Physical investigation

Figure 1 displays the XRD for the glass samples. There were no peaks discovered; instead, a broad hump in the XRD confirmed that the glass samples were amorphous [14, 15].

Figure 2 shows ρ & V_m values of the fabricated samples. As the amount of MoO_3 in the sample increased, the density increased. This is because MoO_3 (143.938 g mole⁻¹) has a higher density and molecular weight than CdO (128.41 g mole⁻¹). The value of V_m declined as MoO_3 increased, as displayed in Fig. 2. This could be due to changes in the glass structure, such as a reduction in bond length between the glass network's structure [16, 17].

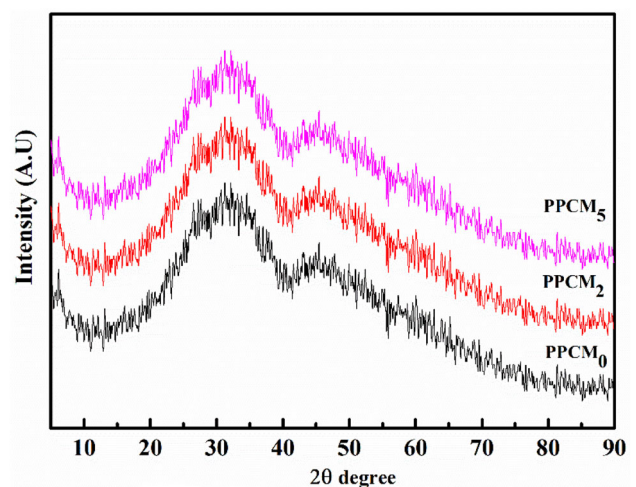


Fig. 1 XRD of fabricated glasses

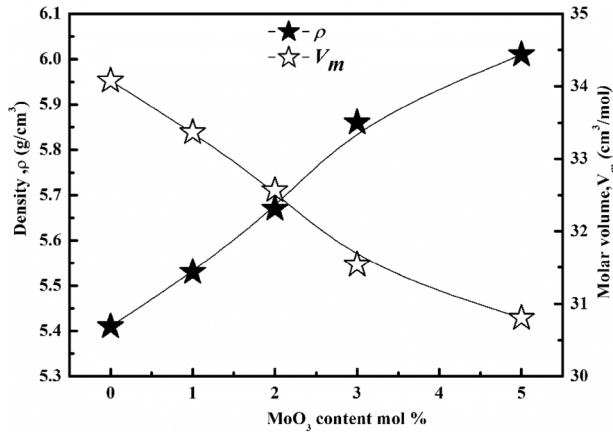


Fig. 2 Density and molar volume of fabricated glasses

3.2 Optical measurements

Figure 3 demonstrates the variation in UV–Vis absorbance of fabricated glasses in the 200–1200 nm range. As a result, the growth of BO is attributed to MoO₃. The absorbance coefficient (α) of the prepared glasses [18–24] is displayed in Fig. 4.

Energy bandgap E_{opt} was estimated using absorption UV–Vis regions by $(\alpha \cdot hv)^{1/2} = B(hv - E_{opt.})$, B is a constant that is not affected by energy. To calculate the indirect E_{opt} from the intercept, plot $(\alpha \cdot hv)^{1/2}$ against hv as is shown in Fig. 5. Because oxygen bridges (BO) are established, which bind excited electrons more strongly than non-bridging oxygen, (NBO) E_{opt} increases with the increase in MoO₃ as shown in Table 2. As shown in Fig. 6 Urbach energy has been calculated as $\propto_0 \exp\left(\frac{hv}{E_u}\right)$. Figure 7 depicts the E_{opt} and E_u values.

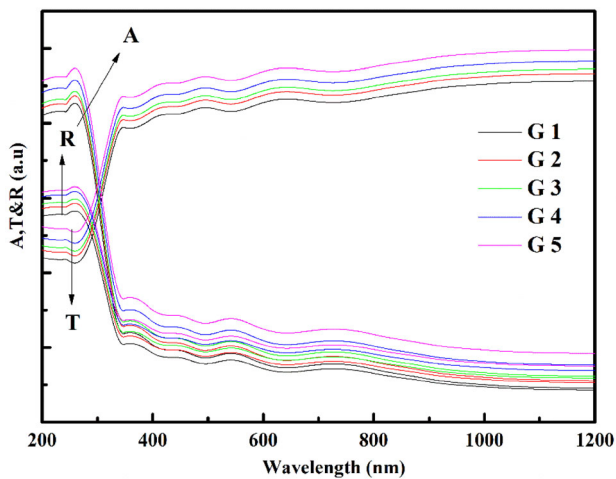


Fig. 3 UV–Vis of fabricated glasses

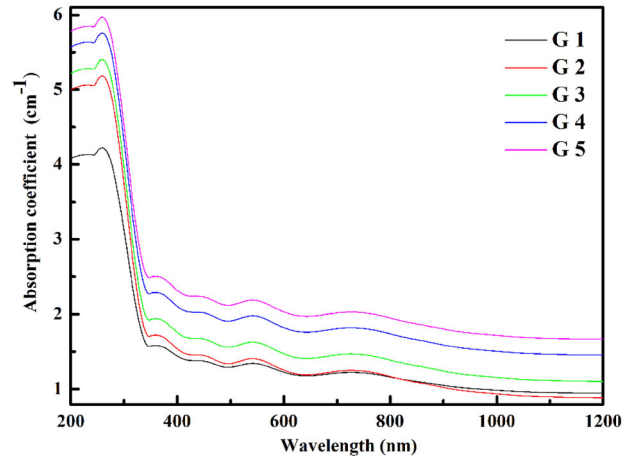


Fig. 4 Absorbance coefficient of fabricated glasses

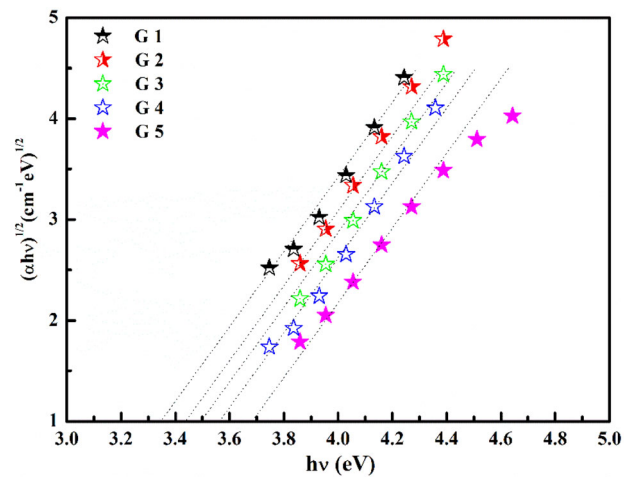


Fig. 5 Plot of $(\alpha hv)^{1/2}$ against (hv) to estimate the bandgap

According to these findings, increasing the amount of MoO₃ has a significant impact on the E_{opt} and E_u . The values of E_{opt} and E_u are presented in Table 2.

Table 2 Optical parameter values

Code	G1	G2	G3	G4	G5
E_{opt}	3.35	3.44	3.51	3.58	3.71
E_u	0.69	0.61	0.59	0.57	0.56
E_o	4.98	4.96	4.715	4.99	5.07
E_d	4.29	4.44	4.62	4.88	5.07
E_{opt}	2.145	2.219	2.31	2.44	2.534
n_o	1.36	1.38	1.407	1.406	1.414
ϵ_∞	1.86	1.90	1.98	1.98	2
So	1.95	2.06	2.08	2.081	2.084
λ	415	477	498	522	558

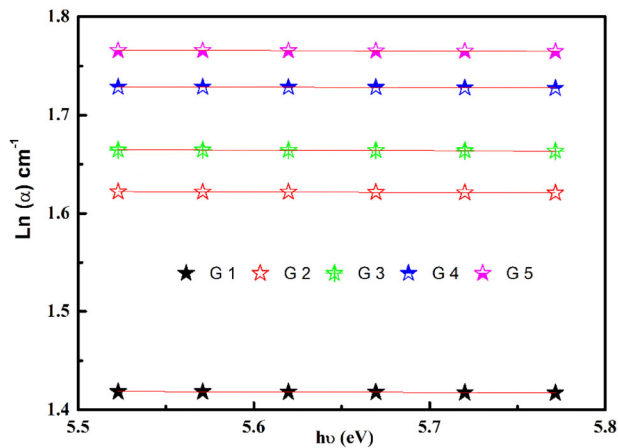


Fig. 6 Plot of $\ln(\alpha)$ absorbance coefficient against $(h\nu)$ to estimate Urbach energy

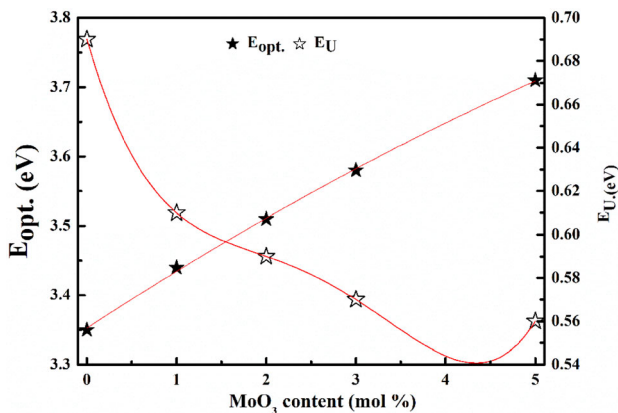


Fig. 7 Bandgap and Urbach energy against MoO_3

The refractive index of fabricated glass was determined by using the following formula: $n_D = \frac{(1-R)^2 + k^2}{(1+R)^2 + k^2}$, $k = \alpha\lambda/4\pi$. n_D of fabricated glasses is shown in Fig. 8. n_D of these glasses increases as density rises, as previously stated.

The following formulas were used to calculate molar polarization R_m , polarizability α_0^{2-} , and optical basicity Λ of glasses: $R_m = \langle n^2 - 1 | n^2 + 2 \rangle V_m$, $\alpha_m = (3|4\pi N)R_m$, and $\alpha_0^{2-} = \frac{V_m \left(\frac{n^2-1}{n^2+2} \right) - \sum \alpha_{cat}}{n_0^{2-}}$ and $\Lambda = 1.67 \left(1 - \frac{1}{\alpha_0^{2-}} \right)$. Figures 9, 10, and 11 show the R_m , α_0^{2-} , and Λ of these glasses, respectively. As the n_D increases these variables increase. Therefore, n_D and R_m , α_0^{2-} , and Λ have a similar trend.

The dispersion of E_o and E_d were estimated by Wemple and Didomenico [25] as $n^2 - 1 = \frac{E_o E_d}{E_0^2 - E^2}$. As shown in Fig. 12, the plotting of $(n^2 - 1)^{-1}$ with $(h\nu)^2 E_o$

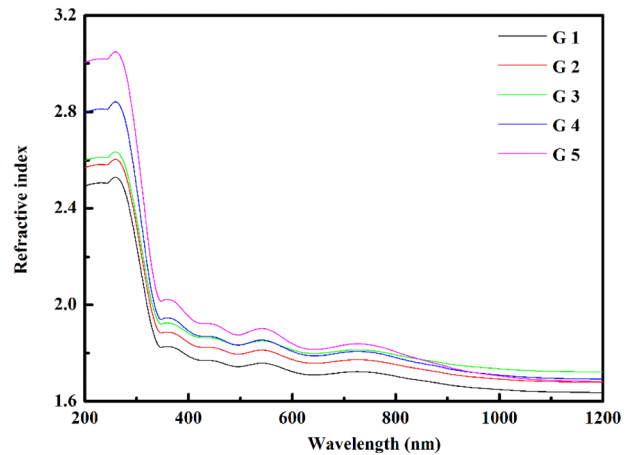


Fig. 8 Refractive index for fabricated glasses

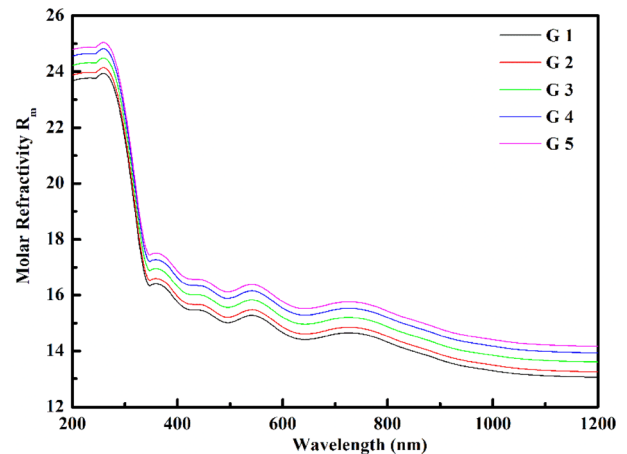


Fig. 9 Molar refractivity for fabricated glasses

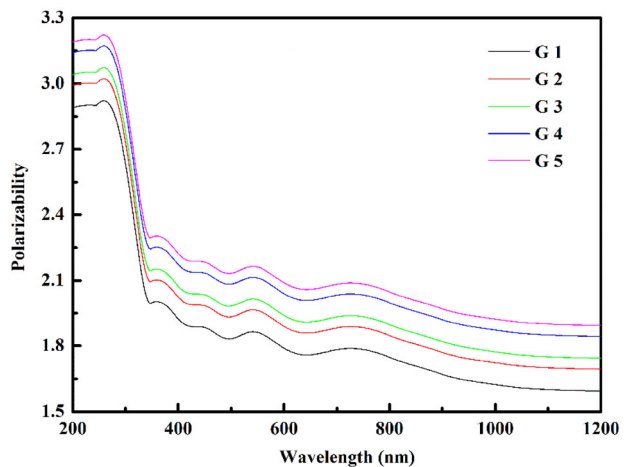


Fig. 10 Polarizability for fabricated glasses

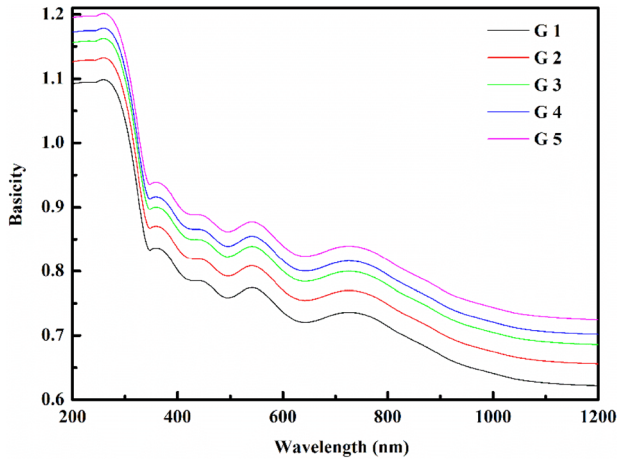


Fig. 11 Optical basicity for fabricated glasses

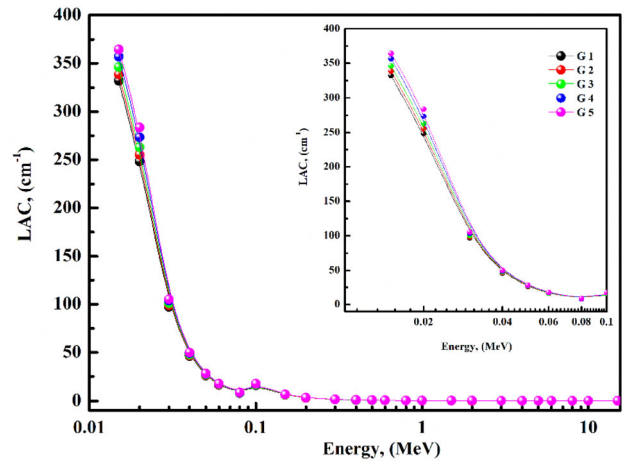


Fig. 14 Linear attenuation coefficient for fabricated glasses

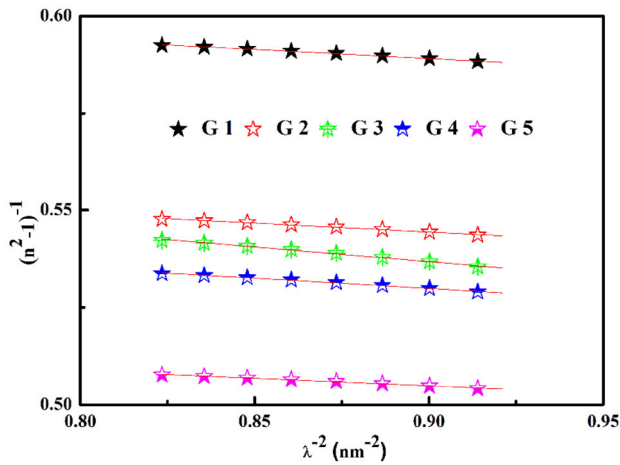


Fig. 12 $(n^2-1)^{-1}$ against $(hv)^{-2}$

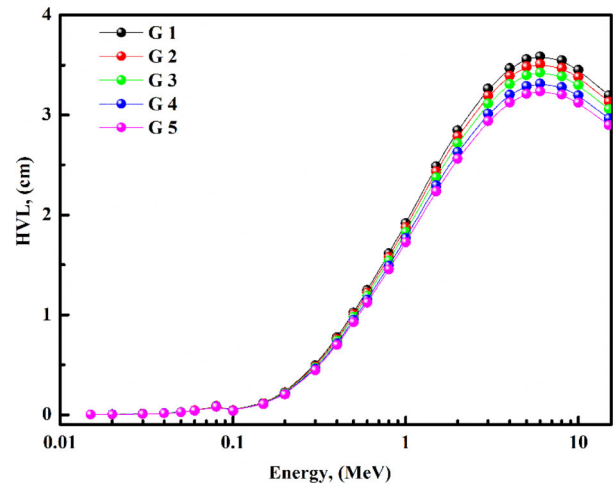


Fig. 15 Half-value layer for fabricated glasses

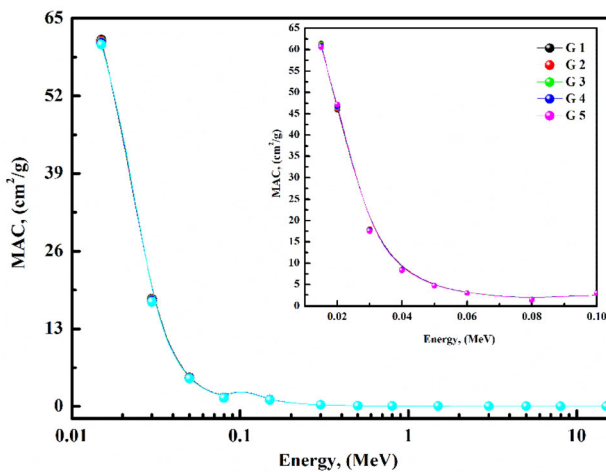


Fig. 13 Mass attenuation coefficient for fabricated glasses

and E_d was calculated from the slope and intercept. A list of these values can be found in Table 2. With the increase in Mo^{3+} , E_o and E_d have been slightly increased. The optical energy E_{opt} represents $E_{opt} = \frac{E_d}{2}$. Refractive Static index at an infinite wavelength (n_o) was estimated by $n_o = \sqrt{1 + \frac{E_d}{E_o}}$ and the static dielectric $\epsilon_\infty = n_o^2$. The oscillator's wavelength (λ_o) and strength (S_o) were calculated using the following formula: $n^2 - 1 = \frac{S_o \lambda_o^2}{1 - (\frac{\lambda_o}{\lambda})^2}$. Table 2 lists the available items.

3.3 Shielding properties

In this study, the radiation attenuation capacities of five different glass samples were assessed. Figure 13

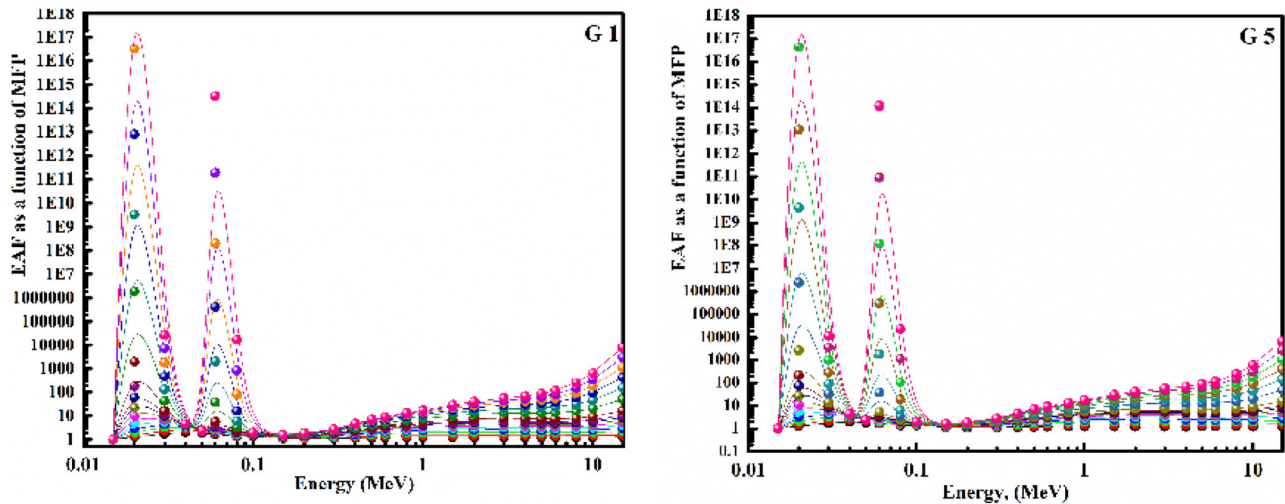


Fig. 16 EBF variation of G1 & G5

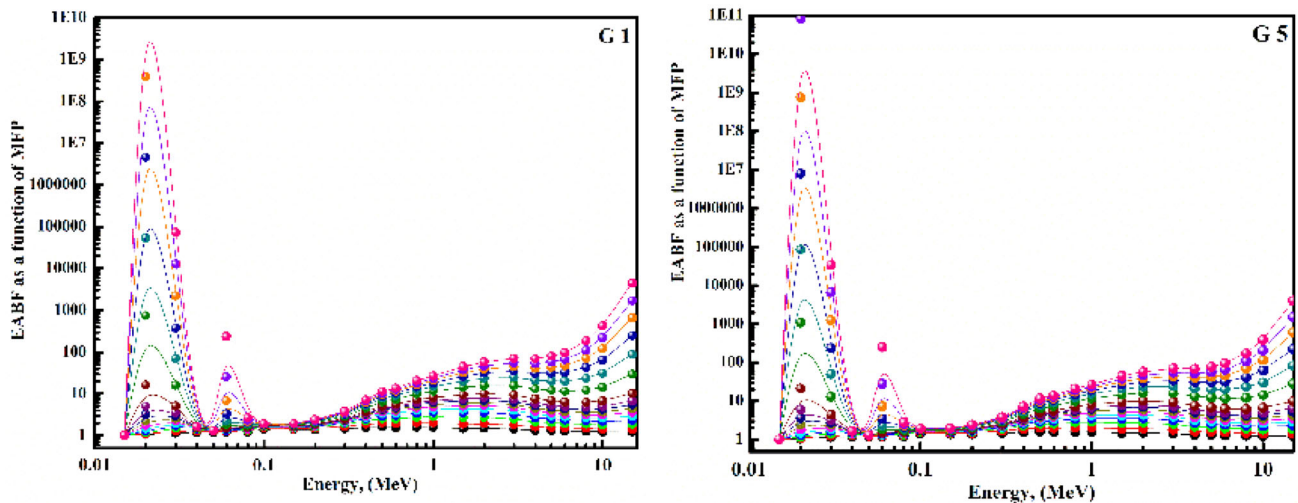


Fig. 17 EABF variation of G1 & G5

depicts the MAC of the fabricated glasses as a function of photon energy. Furthermore, the MAC trend with photon energy in the range in MeV is readily apparent (0.015 to 15). As shown in Fig. 13, the MAC values decrease as photon energy increases. With an increase in the MoO_3 ratio, it is more obvious that the MAC values decrease. In the intermediate photon energy zone, there is a stable or slightly changing behavior, while in the maximum photon energy zone, there is an increase in the MAC values. The photoelectric effect, Compton effect, and pair production effect, and cross-sections in the low, intermediate, and high energy zones, respectively, can be discussed [2, 26–32].

Figure 14 shows the LAC plotted. The photon interaction probability per unit length of the absorber material or medium, measured in cm^{-1} , was illustrated by LAC. As shown in Fig. 14, the LAC values decrease as photon energy increases and increase with the increase of MoO_3 . This increase is due to an increase in the density of the glasses. As a result, the LAC values increased, indicating an inverse trend for glasses.

The HVL parameter is inversely proportional to LAC and defines the shield, absorber, or medium thickness that attenuates or absorbs 50% of the incident intensity. The sample with the lowest HVL has the greatest shielding capacity. As a result of this behavior, G1 is predicted to have the maximum HVL,

while G5 will have the minimum. Among all fabricated glasses, G5 appeared to be the greatest material for shielding. As shown in Fig. 15, the trend $(G1) > (G2) > (G3) > (G4) > (G5)$ ensured the best shielding capacity for fabricated glasses among all other glasses.

Finally, exposure and energy absorption build-up factors are the final parameters that demonstrate the effectiveness of the tested glasses (EBF and EABF). Figures 16 and 17 show the plots of both parameters. With the substitution of CdO for MoO₃, the two parameters have a slight difference. The EBF and EABF were slightly reduced when the MoO₅ molar ratios were increased from 0 to 5. This finding could be linked to or attributed to the investigated substance's effective atomic number. Furthermore, by increasing the MFP from 1 to 40 for all synthesized glasses, the two parameters introduced an increase in their values. The gamma photon energy has an impact on these parameters as well. As a result, the EBF and EABF variance behavior is primarily influenced by the three main interaction mechanisms discussed in the MAC section.

4 Conclusions

For optical and radiation shielding applications, the current study prepared and characterized lead cadmium phosphate glasses doped with different concentrations of MoO₃. We replaced CdO with MoO₃ during this study, which increased density and n_D but a decrease in molar volume. UV–Vis spectroscopy has been used to evaluate the optical characteristics of fabricated glasses. E_{opt} values for the investigated glasses have increased while the E_u values have decreased. As the n_D increase R_m , \propto_0^{2-} , and Λ were increased. The values of fabricated sample dispersion parameters related to n_D were determined. Phy-X/PSD was used to investigate the radiation shielding properties. MAC values improve as the MoO₃ ratio rises. G1 has the maximum HVL value, whereas G5 has the minimum. The exposure and energy absorption build-up factor (EBF and EABF) values decreased slightly as the MoO₃ content increased. As a result, among all other glasses, G5 glasses have the best shielding capacity.

Acknowledgements

We would like to thank Taif University Research Supporting Project number (TURSP-2020/24), Taif University, Taif, Saudi Arabia. Moreover, the authors express their gratitude to the Deanship of Scientific Research at King Khalid University for funding this work through research groups program under Grant Number R.G.P. 2/137/42.

Author contributions

All the authors have accepted full responsibility for the content of this manuscript and have given their approval to its submission.

Declarations

Conflict of interest The authors declare that they have no known competing financial interests.

Consent to participate & publication The authors consent to participate & publication.

References

1. J. Šubčík, L. Koudelka, P. Mošner, L. Montagne, B. Revel, I. Gregora, Structure and properties of MoO₃-containing zinc borophosphate glasses. *J. Non-Cryst. Solids* **355**, 970–975 (2009). <https://doi.org/10.1016/j.jnoncrysol.2009.04.017>
2. K.S. Shaaban, H.Y. Zahran, I.S. Yahia, H.I. Elsaedy, E.R. Shaaban, S.A. Makhlof, E.A.A. Wahab, E.S. Yousef, Mechanical and radiation-shielding properties of B₂O₃–P₂O₅–Li₂O–MoO₃ glasses. *Appl. Phys. A* (2020). <https://doi.org/10.1007/s00339-020-03982-9>
3. M.A. Sayed, A.M. Ali, A.F. Abd El-Rehim et al., Dispersion parameters, polarizability, and basicity of lithium phosphate glasses. *J. Electron. Mater.* **50**, 3116–3128 (2021). <https://doi.org/10.1007/s11664-021-08921-9>
4. S.R. Yousefi, M. Ghanbari, O. Amiri, Z. Marzhooseyni, P. Mehdizadeh, M. Hajizadeh-Oghaz, M. Salavati-Niasari, Dy₂BaCuO₅/Ba₄DyCu₃O_{9,09} S-scheme heterojunction nanocomposite with enhanced photocatalytic and antibacterial activities. *J. Am. Ceram. Soc.* **104**, 2952–2965 (2021). <https://doi.org/10.1111/jace.17696>
5. U. Selvaraj, K.J. Rao, Role of lead in lead phosphomolybdate glasses and a model of structural units. *J. Non-Cryst. Solids* **104**, 300–315 (1988). [https://doi.org/10.1016/0022-3093\(88\)90401-2](https://doi.org/10.1016/0022-3093(88)90401-2)

6. E.A. Abdel Wahab, A.A. El-Maaref, K.S. Shaaban, J. Börcsök, M. Abdelawwad, Lithium cadmium phosphate glasses doped Sm^{3+} as a host material for near-IR laser applications. *Opt. Mater.* **111**, 110638 (2021). <https://doi.org/10.1016/j.optmat.2020.110638>
7. S.R. Yousefi, H.A. Alshamsi, O. Amiri, M. Salavati-Niasari, Synthesis, characterization and application of $\text{Co}/\text{Co}_3\text{O}_4$ nanocomposites as an effective photocatalyst for discoloration of organic dye contaminants in wastewater and antibacterial properties. *J. Mol. Liq.* **337**, 116405 (2021). <https://doi.org/10.1016/j.molliq.2021.116405>
8. S.R. Yousefi, A. Sobhani, H.A. Alshamsi, M. Salavati-Niasari, Green sonochemical synthesis of $\text{BaDy}_2\text{NiO}_5/\text{Dy}_2\text{O}_3$ and $\text{BaDy}_2\text{NiO}_5/\text{NiO}$ nanocomposites in the presence of core almond as a capping agent and their application as photocatalysts for the removal of organic dyes in water. *RSC Adv.* **11**, 11500–11512 (2021). <https://doi.org/10.1039/d0ra10288a>
9. K.S. Shaaban, M.S.I. Koubisy, H.Y. Zahran, I.S. Yahia, Spectroscopic properties, electronic polarizability, and optical basicity of titanium-cadmium tellurite glasses doped with different amounts of lanthanum. *J. Inorg. Organomet. Polym. Mater.* **30**, 4999–5008 (2020). <https://doi.org/10.1007/s10904-020-01640-4>
10. S.R. Yousefi, O. Amiri, M. Salavati-Niasari, Control sonochemical parameter to prepare pure $\text{Zn}_{0.35}\text{Fe}_{2.65}\text{O}_4$ nanostructures and study their photocatalytic activity. *Ultrason. Sonochem.* **58**, 104619 (2019). <https://doi.org/10.1016/j.ultsonch.2019.104619>
11. S.R. Yousefi, M. Masjedi-Arani, M.S. Morassaei, M. Salavati-Niasari, H. Moayedi, Hydrothermal synthesis of $\text{DyMn}_2\text{O}_5/\text{Ba}_3\text{Mn}_2\text{O}_8$ nanocomposite as a potential hydrogen storage material. *Int. J. Hydrog. Energy* **44**(43), 24005–24016 (2019). <https://doi.org/10.1016/j.ijhydene.2019.07.113>
12. S.R. Yousefi, A. Sobhani, M. Salavati-Niasari, A new nanocomposite superionic system ($\text{CdHgI}_4/\text{HgI}_2$): synthesis, characterization and experimental investigation. *Adv. Powder Technol.* **28**(4), 1258–1262 (2017). <https://doi.org/10.1016/j.apt.2017.02.013>
13. S.R. Yousefi, D. Ghanbari, M. Salavati-Niasari, M. Hassanpour, Photo-degradation of organic dyes: simple chemical synthesis of $\text{Ni}(\text{OH})_2$ nanoparticles, $\text{Ni}/\text{Ni}(\text{OH})_2$ and Ni/NiO magnetic nanocomposites. *J. Mater. Sci.: Mater. Electron.* **27**(2), 1244–1253 (2016)
14. K.S. Shaaban, I. Boukhris, I. Kebaili, M.S. Al-Buriah, Spectroscopic and attenuation shielding studies on $\text{B}_2\text{O}_3\text{-SiO}_2\text{-LiF-ZnO-TiO}_2$ glasses. *SILICON* (2021). <https://doi.org/10.1007/s12633-021-01080-w>
15. K.S. Shaaban, A.M. Al-Baradi, E.A.A. Wahab, The impact of Y_2O_3 on physical and optical characteristics, polarizability, optical basicity, and dispersion parameters of $\text{B}_2\text{O}_3\text{-SiO}_2\text{-Bi}_2\text{O}_3\text{-TiO}_2$ glasses. *SILICON* (2021). <https://doi.org/10.1007/s12633-021-01309-8>
16. K.H. Mahmoud, A.S. Alsubaie, E.A.A. Wahab, F.M. Abdel-Rahim, K.S. Shaaban, Research on the effects of yttrium on bismuth titanate borosilicate glass system. *SILICON* (2021). <https://doi.org/10.1007/s12633-021-01125-0>
17. A.F.A. El-Rehim, K.S. Shaaban, Influence of La_2O_3 content on the structural, mechanical, and radiation-shielding properties of sodium fluoro lead barium borate glasses. *J. Mater. Sci.: Mater. Electron.* **32**, 4651–4671 (2021). <https://doi.org/10.1007/s10854-020-05204-7>
18. K.S. Shaaban, S. Alomairy, M.S. Al-Buriah, Optical, thermal and radiation shielding properties of $\text{B}_2\text{O}_3\text{-NaF-PbO-BaO-La}_2\text{O}_3$ glasses. *J. Mater. Sci.: Mater. Electron.* (2021). <https://doi.org/10.1007/s10854-021-05885-8>
19. A.A. El-Maaref, E.A.A. Wahab, K.S. Shaaban, R.M. El-Agmy, Enhancement of spectroscopic parameters of Er^{3+} -doped cadmium lithium gadolinium silicate glasses as an active medium for lasers and optical amplifiers in the NIR-region. *Solid State Sci.* **113**, 106539 (2021). <https://doi.org/10.1016/j.solidstatesciences.2021.106539>
20. A.F.A. El-Rehim, A.M. Ali, H.Y. Zahran, I.S. Yahia, K.S. Shaaban, Spectroscopic, structural, thermal, and mechanical properties of $\text{B}_2\text{O}_3\text{-CeO}_2\text{-PbO}_2$ glasses. *J. Inorg. Organomet. Polym. Mater.* **31**, 1774–1786 (2021). <https://doi.org/10.1007/s10904-020-01799-w>
21. S. Alomairy, A.M. Aboraia, E.R. Shaaban, K.S. Shaaban, Comparative studies on spectroscopic and crystallization properties of $\text{Al}_2\text{O}_3\text{-Li}_2\text{O-B}_2\text{O}_3\text{-TiO}_2$ glasses. *Braz. J. Phys.* **51**, 1237–1248 (2021). <https://doi.org/10.1007/s13538-021-00928-1>
22. A.M. Al-Baradi, A.F.A. El-Rehim, Z.A. Alrowaili, M.S. Al-Buriah, K.S. Shaaban, FT-IR and gamma shielding characteristics of $22\text{SiO}_2\text{-}23\text{Bi}_2\text{O}_3\text{-}37\text{B}_2\text{O}_3\text{-}13\text{TiO}_2\text{-(5-x) LiF-x BaO}$ glasses. *SILICON* (2021). <https://doi.org/10.1007/s12633-021-01481-x>
23. E.A.A. Wahab, A.M. Aboraia, A.M.E. Shafey, K.S. Shaaban, A.V. Soldatov, The effect of ZrO_2 on the linear and non-linear optical properties of sodium silicate glass. *Opt. Quant. Electron.* (2021). <https://doi.org/10.1007/s11082-021-03164-8>
24. E.A. Abdel Wahab, K.S. Shaaban, S. Alomairy, M.S. Al-Buriah, Electronegativity and optical basicity of glasses containing Na/Pb/B and their high performance for radiation applications: role of ZrO_2 nanoparticles. *Eur. Phys. J. Plus* (2021). <https://doi.org/10.1140/epjp/s13360-021-01572-z>
25. S.H. Wemple, M. DiDomenico Jr., Behavior of the electronic dielectric constant in covalent and ionic materials. *Phys. Rev. B* **3**, 1338–1351 (1971). <https://doi.org/10.1103/PhysRevB.3.1338>

26. E. Şakar, Ö.F. Özpolat, B. Alim, M.I. Sayyed, M. Kurudirek, PhyX/PSD: development of a user-friendly online software for calculation of parameters relevant to radiation shielding and dosimetry. *Radiat. Phys. Chem.* **166**, 108496 (2020). <https://doi.org/10.1016/j.radphyschem>
27. M.A. Alothman, Z.A. Alrowaili, J.S. Alzahrani, E.A.A. Wahab, I.O. Olarinoye, C. Sriwunkum, K.S. Shaaban, M.S. Al-Buriahi, Significant influence of MoO₃ content on synthesis, mechanical, and radiation shielding properties of B₂O₃-Pb₃O₄-Al₂O₃ glasses. *J. Alloys Compd.* **882**, 160625 (2021). <https://doi.org/10.1016/j.jallcom.2021.160625>
28. S. Alomairy, Z.A. Alrowaili, I. Kebaili, E.A.A. Wahab, C. Mutuwong, M.S. Al-Buriahi, K.S. Shaaban, Synthesis of Pb₃O₄-SiO₂-ZnO-WO₃ glasses and their fundamental properties for gamma shielding applications. *SILICON* (2021). <https://doi.org/10.1007/s12633-021-01347-2>
29. B. Albarzan, A.H. Almuqrin, M.S. Koubisy, E.A. Abdel Wahab, K.A. Mahmoud, Kh.S. Shaaban, M.I. Sayyed, Effect of Fe₂O₃ doping on structural, FTIR and radiation shielding characteristics of aluminium-lead-borate glasses. *Prog. Nucl. Energy* **141**, 103931 (2021). <https://doi.org/10.1016/j.pnuce.2021.103931>
30. A.F.A. El-Rehim, H.Y. Zahran, I.S. Yahia, S.A. Makhlof, K.S. Shaaban, Radiation, crystallization, and physical properties of cadmium borate glasses. *SILICON* **13**, 2289–2307 (2021). <https://doi.org/10.1007/s12633-020-00798-3>
31. A.F.A. El-Rehim, H.Y. Zahran, I.S. Yahia, A.M. Ali, K.S. Shaaban, Physical, radiation shielding and crystallization properties of Na₂O-Bi₂O₃-MoO₃-B₂O₃-SiO₂-Fe₂O₃ Glasses. *SILICON* (2020). <https://doi.org/10.1007/s12633-020-00827-1>
32. A.M. Fayad, K.S. Shaaban, W.M. Abd-Allah, M. Ouis, Structural and optical study of CoO doping in borophosphate host glass and effect of gamma irradiation. *J. Inorg. Organomet. Polym. Mater.* **30**, 5042–5052 (2020). <https://doi.org/10.1007/s10904-020-01641-3>

Publisher's Note Springer Nature remains neutral with regard to jurisdictional claims in published maps and institutional affiliations.